SOLUTIONS FOR INCOMPRESSIBLE SEPARATED BOUNDARY LAYERS INCLUDING VISCOUS-INVISCID INTERACTION

By James E. Carter and Stephen F. Wornom
NASA Langley Research Center

SUMMARY

Numerical solutions are presented for the laminar and turbulent boundary-layer equations for incompressible flows with separation and reattachment. The separation singularity is avoided by using an inverse technique in which the displacement thickness is prescribed and the pressure is deduced from the resulting solution. The turbulent results appear qualitatively correct despite the use of a two-layer eddy-viscosity model which is generally assumed appropriate only for mild-pressure-gradient flows. A new viscous-inviscid interaction technique is presented in which the inviscid flow is solved inversely by prescribing the pressure from the boundary-layer solution and deducing the new displacement thickness from the solution of a Cauchy integral. Calculations are presented using this interaction procedure for a laminar flow in which separation and reattachment occur on a solid surface.

INTRODUCTION

The development of theoretical prediction techniques for flows involving boundary-layer separation is of fundamental importance since separation is a common occurrence on most aerodynamic surfaces. Significant progress has been made in recent years for laminar supersonic flows which contain large viscous-inviscid interactions, such as those which occur at the point of incidence of a shock wave on a flat plate or in the vicinity of a compression corner. Werle and Vatsa (ref. 1) and Dwoyer (ref. 2), as well as others, have demonstrated that the boundary-layer equations including interaction with the inviscid flow provide an accurate model which gives results that agree with experiment and solutions of the Navier-Stokes equations (ref. 3). In addition these techniques are currently being extended to turbulent flows (ref. 4).

In supersonic flows the interaction between the viscous and inviscid flow can be computed locally since the inviscid flow is hyperbolic. As a result the singularity which occurs in solutions of the boundary-layer equations when the pressure is prescribed is removed by allowing the boundary layer to modify the pressure to give a regular solution at the separation point. This technique cannot be used for subsonic flows since the invis-

cid flow is elliptic and hence, the pressure at any given point depends on the entire displacement body distribution.

Alternate procedures which are appropriate for subsonic flows and do not rely on interaction to eliminate the separation singularity are the inverse boundary-layer solution techniques which have been recently developed. Catherall and Mangler (ref. 5), and later Carter (ref. 6), have demonstrated that regular solutions can be obtained if the displacement thickness is prescribed and the pressure is deduced from the resulting solution. Similarly, regular solutions at separation can be obtained by prescribing the skin friction as shown by Kuhn and Nielsen (ref. 7), Klineberg and Steger (ref. 8), and Carter (ref. 6). Another inverse procedure, which was developed earlier by Klineberg and Steger (ref. 9) and later used by Tai (ref. 10), is to use the transverse component of velocity at the boundary-layer edge as the prescribed condition.

In contrast with these inverse techniques, Briley and McDonald (ref. 11) have made calculations for subsonic flow using a direct procedure in which the unsteady boundary-layer equations are repeatedly solved until a steady-state solution is obtained. After each time step the prescribed pressure is updated from thin airfoil theory, thereby accounting for the displacement thickness interaction. Although this technique seems feasible, it needs further examination since Briley and McDonald obtained a regular solution at a laminar separation point for a case with no interaction. The absence of the singularity in this case is probably due to numerical inaccuracy since a first-order scheme was used with a coarse grid. Hence, it is not clear in those cases in which interaction was included whether the solution at separation would be regular if a second-order scheme were used.

In using the inverse boundary-layer procedures discussed above, it is necessary to incorporate a description of the inviscid flow to completely describe a viscous-inviscid interaction. For example, Kuhn and Nielsen (ref. 7) developed an iterative procedure in which Murman's inviscid transonic flow program (ref. 12) is solved iteratively with their inverse boundary-layer technique. Kuhn and Nielsen made calculations for the turbulent separated flow behind a bump placed on a wind-tunnel wall. The skin friction was updated for each new boundary-layer calculation based on the difference between the pressure computed from the boundary-layer solution and that obtained from the inviscid flow calculation for the displacement body. This procedure is not straightforward as it is not clear how to update the skin friction based on this pressure mismatch. A simpler procedure, which was recommended by Kuhn and Nielsen and is the subject of the present paper, is to combine the displacement-thickness-prescribed, inverse boundary-layer procedure with a suitable representation of the inviscid flow. In the present study of incompressible flow, the inviscid calculations are made by using an inverse Cauchy integral from thin airfoil theory.

The Cauchy integral relating pressure and body slope is used in an inverse manner so that a new displacement body can be found from the pressure obtained in the inverse boundary-layer calculation. The displacement thickness is then updated by subtracting the prescribed body from the displacement body and the iteration is continued to convergence. This procedure is similar to that used by Jobe and Burggraf (ref. 13) and by Melnik and Chow (ref. 14) in solving the asymptotic equations developed by Stewartson (ref. 15) governing the flow at the trailing edge of a flat plate. An important feature of this inverse procedure is that the results require no smoothing, as has been typically found necessary in direct calculations of inviscid-viscous interaction (refs. 16 and 17). This result is not surprising since the inverse procedure primarily uses numerical integration, which is inherently a smoothing process, in contrast to the numerical differentiation used in the direct procedure.

A second purpose of this paper is to present some calculations which have been made for turbulent flows involving separation and reattachment. These calculations, which do not include interaction, have been made by incorporating a two-layer eddy-viscosity model in the displacement-thickness-prescribed procedure used in the laminar analyses. The variable grid scheme analyzed by Blottner (ref. 18) is incorporated in these calculations to reduce the number of grid points across the boundary layer and simultaneously maintain second-order accuracy.

SYMBOLS

$A_n, B_n,$ C_n, D_n	coefficients in tridiagonal system of equations
C_n', D_n'	coefficients in Thomas algorithm
C_f	skin-friction coefficient
C_p	pressure coefficient
L	reference length
ℓ	coefficient in vorticity-transport equation (see eqs. (1) and (8))
m, n	indices for ξ- and η-directions, respectively
N	computational coordinate

ΔN	increment in computational coordinate
$R_{\infty,L}$	free-stream Reynolds number, $\left(\dfrac{\rho U L}{\mu}\right)_{\infty}$
R	reattachment point
S	separation point
t	thickness (see fig. 3)
U_{∞}	free-stream velocity
u	velocity component parallel to surface
u_e	velocity component parallel to surface at edge of boundary layer
$u'v'$	Reynolds stress component
x	coordinate along surface
Δx	increment in coordinate along surface
x_0	upstream interaction boundary
x_1	downstream interaction boundary
x'	integration variable
y	coordinate normal to surface
α	coefficient of artificial time term
Δ	increment in displacement thickness
δ	boundary-layer thickness
δ^*	displacement thickness
$\bar{\delta}^*$	$= \delta^* \sqrt{R_{\infty,L}}$

ϵ eddy-viscosity coefficient

η transformed y-coordinate

$\Delta\eta$ grid spacing in η-direction

μ molecular viscosity coefficient

ν kinematic coefficient of viscosity

ξ transformed x-coordinate

$\Delta\xi$ grid spacing in ξ-direction

ρ density

ψ stream function

$\overline{\psi}$ $= \psi\sqrt{R_{\infty,L}}$

$\tilde{\psi}$ transformed stream function

ω vorticity

$\overline{\omega}$ $= \omega\Big/\sqrt{R_{\infty,L}}$

Subscripts:

B   body

DB   displacement body

FP   flat plate

max   maximum

o   denotes value at upstream boundary

tr   transition

Governing Equations

The governing equations for an incompressible boundary-layer flow for a prescribed displacement thickness can be given in terms of the following vorticity-transport and stream-function equations:

$$u\bar{\delta}^{*2}\frac{\partial\overline{\omega}}{\partial\xi} - \bar{\delta}^*\left\{\frac{\partial}{\partial\xi}\left[\tilde{\psi} + (\eta - 1)\left(u\bar{\delta}^*\right)\right]\right\}\frac{\partial\overline{\omega}}{\partial\eta} = \frac{\partial^2\ell\overline{\omega}}{\partial\eta^2} \tag{1}$$

$$\frac{\partial\tilde{\psi}}{\partial\eta} = \bar{\delta}^{*2}(1 - \eta)\overline{\omega} \tag{2}$$

These equations are solved subject to the boundary conditions

$$u(\xi,0) = \tilde{\psi}(\xi,0) = 0 \tag{3}$$

$$\overline{\omega}(\xi,\eta) \text{ and } \tilde{\psi}(\xi,\eta) \to 0 \text{ as } \eta \to \infty \tag{4}$$

The independent variables are $\xi = x$ and $\eta = y/\bar{\delta}^*$ where $\bar{\delta}^*$ is the displacement thickness which is defined in the usual manner. Equations (1) and (2) are nondimensional and the dependent variables which are barred have been scaled in the usual manner by $\sqrt{R_{\infty,L}}$ which is appropriate for laminar boundary layers. The transformed stream function $\tilde{\psi}$ is related to the usual stream function $\overline{\psi}$ by $\tilde{\psi} = \overline{\psi} - u\bar{\delta}^*(\eta - 1)$ where u is the x-component of velocity. The vorticity is denoted by $\overline{\omega}$ and after it is obtained from equation (1), u is given by

$$u(\xi,\eta) = \bar{\delta}^* \int_0^\eta \overline{\omega}\left(\xi,\eta_1\right)d\eta_1 \tag{5}$$

After equations (1), (2), and (5) are solved, the unknown edge velocity u_e is obtained from the x-momentum equation which is evaluated at the surface to give

$$u_e\frac{du_e}{d\xi} = -\frac{1}{\bar{\delta}^*}\frac{\partial\overline{\omega}}{\partial\eta}\bigg|_{\eta=0} \tag{6}$$

This value should agree with the value obtained from equation (5) and thus serves as a check on the calculation. Equation (6) is integrated from the upstream boundary to give $u_e(\xi)$ and the corresponding pressure coefficient is given by

$$C_p = 1 - u_e{}^2 \qquad (7)$$

Further details of the preceding formulation for laminar flow are presented by Carter (ref. 6).

For laminar flows the quantity ℓ appearing in equation (1) is set equal to unity, whereas for turbulent flow

$$\ell = 1 + \frac{\epsilon}{\mu} \qquad (8)$$

where ϵ/μ is the ratio of the eddy viscosity to the molecular viscosity coefficient. The eddy-viscosity coefficient is used to relate the Reynolds stress to the velocity gradient in the usual manner

$$\overline{\rho u'v'} = -\epsilon \frac{\partial u}{\partial y} \qquad (9)$$

In the present calculations a two-layer eddy-viscosity formulation has been used which is similar to that used by Harris (ref. 19), Cebeci and Keller (ref. 20), and others. In the inner region a combination of Prandtl's mixing length model along with the Van Driest damping factor is used and is given as follows in dimensional quantities:

$$\left(\frac{\epsilon}{\mu}\right)_{inner} = \frac{(0.4yD)^2}{\nu}\left|\frac{\partial u}{\partial y}\right| \qquad (10)$$

where the damping factor D has been modified for separated flows and is given by

$$D = 1 - \exp\left[-\frac{y}{26}\sqrt{\left|\frac{1}{\nu}\left|\frac{\partial u}{\partial y}\right|\right|_{max}}\right] \qquad (11)$$

In the outer region Clauser's velocity defect model is used along with the Klebanoff intermittency factor

$$\left(\frac{\epsilon}{\mu}\right)_{outer} = \frac{0.0168u_e\delta^*}{\nu}\left[\frac{1}{1 + 5.5(y/\delta)^6}\right] \qquad (12)$$

where δ is the boundary-layer thickness defined as the point where $u = 0.995u_e$. The boundary between the inner and outer regions is the point at which

131

$$\left(\frac{\epsilon}{\mu}\right)_{inner} = \left(\frac{\epsilon}{\mu}\right)_{outer} \qquad (13)$$

Equations (10) to (13) relate the Reynolds stress to the mean flow and thereby complete the formulation for turbulent flows. This two-layer eddy-viscosity model has been widely used for attached flows with mild pressure gradients; its applicability to separated turbulent flows is unknown at the present time. Nonetheless, the purpose of the present paper is to develop a numerical scheme for separated turbulent flows; in the future, refinements of the turbulent empiricism will be made to assess the quantitative results in comparison with experiment.

Numerical Procedure

Figure 1 gives a schematic diagram of the computational schemes and boundary conditions used for the boundary-layer calculations. In an earlier paper Carter (ref. 6) presented a global iteration procedure in which the finite-difference scheme is switched in the reversed-flow region to properly account for the reversed-flow direction. The global iteration technique requires repeated streamwise iterations until convergence is obtained. More recently, Carter and Wornom (ref. 21) have shown that a separated boundary layer can be computed much more rapidly with the usual forward-marching procedure used for attached boundary layers provided that the tridiagonal equations are diagonally dominant and that the streamwise convection of vorticity is neglected in the reversed-flow region; that is, if $u < 0$, then set

$$\bar{u}\delta^{*2}\frac{\partial\bar{\omega}}{\partial\xi} = 0 \qquad (14)$$

This approximation is somewhat similar to that used by Reyhner and Flügge-Lotz (ref. 22) for neglecting the streamwise convection of momentum in the reversed-flow region. Use of this approximation eliminates the well-known instability of marching in a direction opposite to that of the flow; in addition, the accuracy is essentially unaffected if the magnitude of the reversed-flow velocity is less than $0.1U_\infty$, as shown by Carter and Wornom (ref. 21).

The streamwise gradients which are typically encountered as a boundary layer approaches separation are quite large, and thus, from numerical experimentation it has been found necessary to use a fully second-order-accurate scheme for $u > 0$. The Crank-Nicolson scheme, including the reversed-flow approximation discussed previously, is used in the laminar calculations and has been previously discussed in references 6 and 21. The turbulent forward-marching procedure, which is presented subsequently, is quite similar although the computational molecule shown in figure 1 is used since the

Crank-Nicolson scheme resulted in oscillatory solutions for some of the turbulent calculations. In this case the streamwise derivatives are represented by the second-order difference expression

$$\frac{\partial \omega}{\partial \xi}\bigg|_{m,n} = \frac{1}{2\,\Delta\xi}\Big(3\omega_{m,n} - 4\omega_{m-1,n} + \omega_{m-2,n}\Big) \tag{15}$$

The bars, which were used previously to denote Reynolds number scaling, are deleted for convenience in the presentation of the numerical procedure. The computational molecule for $u < 0$ in the global turbulent calculation is the same as that reported for laminar flow by Carter (ref. 3). A constant grid spacing is used in the stream direction and hence $\xi = m\,\Delta\xi$. In the normal direction a variable grid is used, second-order accuracy being maintained by using the difference expressions developed by Blottner (ref. 18) which are given as

$$\frac{\partial \omega}{\partial \eta}\bigg|_{m,n} = \frac{\omega_{m,n+1} - \omega_{m,n-1}}{\eta_{n+1} - \eta_{n-1}} + O(\Delta N^2) \tag{16}$$

$$\frac{\partial^2 \ell\omega}{\partial \eta^2}\bigg|_{m,n} = \frac{2}{\eta_{n+1} - \eta_{n-1}}\left[\frac{(\ell\omega)_{m,n+1} - (\ell\omega)_{m,n}}{\eta_{n+1} - \eta_n} - \frac{(\ell\omega)_{m,n} - (\ell\omega)_{m,n-1}}{\eta_n - \eta_{n-1}}\right] + O(\Delta N^2) \tag{17}$$

Blottner showed that a variable grid scheme is equivalent to a coordinate stretching method if the coordinate η can be related to a computational coordinate N in which the grid is evenly spaced. In the present calculations the grid is varied at a constant rate; that is, $\Delta\eta_n = K\,\Delta\eta_{n-1}$, which can be written in terms of a computational coordinate N as follows

$$\eta_n = \eta_{max}\frac{K^{N_n/\Delta N} - 1}{K^{1/\Delta N} - 1} \tag{18}$$

where $N_n = (n-1)\Delta N$ and $0 \leq N \leq 1$. In the present calculations K, the ratio of adjacent grid spacings, equals 1.09, $\eta_{max} = 31$, and 93 grid points are used across the boundary layer. This grid point distribution insures a minimum of 15 points in the viscous sublayer. However, no numerical study was made to determine the optimum value of K or the minimum number of grid points. By using equations (15) to (17) the vorticity transport equation can be written in the following form where q denotes the column iteration level:

$$A_n^q \omega_{m,n-1}^{q+1} + \left(B_n + \alpha\right)^q \omega_{m,n}^{q+1} + C_n^q \omega_{m,n+1}^{q+1} = D_n^q + \alpha \omega_{m,n}^q \tag{19}$$

where

$$A_n = -\left(C_\eta + K\ell_{m,n-1}\right)$$

$$B_n = (K + 1)\ell_{m,n} + 3C_\xi$$

$$C_n = C_\eta - \ell_{m,n+1}$$

$$D_n = C_\xi\left(4\omega_{m-1,n} - \omega_{m-2,n}\right)$$

$$C_\xi = K(K + 1)\left(\delta_m^* \, \Delta\eta_{n-1}\right)^2 \frac{u_{m,n}}{4\,\Delta\xi} \tag{20}$$

$$C_\eta = -\frac{K\delta_m^* \, \Delta\eta_{n-1}}{2} \frac{\partial}{\partial\xi}\left[\tilde{\psi} + (\eta - 1)(u\delta^*)\right]\Bigg|_{m,n}$$

$$\alpha = 2\left|C_\eta\right| + \ell_{m,n+1} + K\ell_{m,n-1} - (K + 1)\ell_{m,n}$$

In the reversed-flow region the streamwise convection of vorticity is neglected; as a result $C_\xi = 0$.

Repeated application of equation (19) from the wall to the outer boundary results in a tridiagonal system of linear equations for the vorticity. These equations are solved by the Thomas algorithm which can be written as

$$\omega_{m,n}^{q+1} = D_n' + C_n' \omega_{m,n-1}^{q+1} \tag{21}$$

where

$$D_n' = \frac{D_n - C_n D_{n+1}'}{B_n + C_n C_{n+1}'} \qquad\qquad C_n' = \frac{-A_n}{B_n + C_n C_{n+1}'} \tag{22}$$

In equation (19) a timelike term $\alpha\left(\omega_{m,n}^{q+1} - \omega_{m,n}^q\right)$ has been introduced to provide the unconditional diagonal dominance

134

$$|B_n + \alpha| \geq |A_n| + |C_n| \qquad\qquad \qquad (23)$$

and thereby prevent error growth in the back substitution procedure given in equation (21). Introduction of this term is a modification of the usual implicit technique used to solve the boundary-layer equations and is the subject of a recent paper by Carter and Wornom (ref. 21).

The quantities D_n' and C_n' are computed, beginning at the outer boundary where the boundary condition $\omega(\xi,\infty) = 0$ is imposed and proceeding to the wall. Equation (21) is then used to obtain $\omega_{m,n}^{q+1}$ once the value at the wall $\omega_{m,1}^{q+1}$ is known. The wall vorticity is found by simultaneously solving for the stream function from equation (2) across the boundary layer and imposing the surface boundary condition given in equation (3). Details of this procedure are the same as those used for laminar flow which are presented by Carter (ref. 6). After the back substitution in equation (21) is completed, the coefficients in equation (19) are updated and the process continued until convergence is obtained. Convergence is assumed when the maximum change in all the dependent variables between two successive column iterations is less than 10^{-5}. In most of the calculations it was necessary to use underrelaxation for the iterative column solution, as was discussed by Carter (ref. 6). The relaxation factor typically used in both the laminar and turbulent calculations was 0.6.

INVISCID FLOW AND INTERACTION PROCEDURE

In this section the inviscid flow, which is approximated by small-disturbance theory, and the interaction procedure shown in figure 2 are discussed. This procedure is applied to the laminar flow over the surface shown schematically in figure 3 in which flow separation and reattachment occur. The strong viscous-inviscid interaction region is assumed to be limited to the region shown in figure 3 in order to replace the infinite limits in the Cauchy integral, which is used to compute the inviscid flow, with finite values. Thus, it is assumed that the region of strong interaction is located a large distance from the leading edge and the Blasius flat-plate displacement thickness at this location results in a negligible pressure gradient. These assumptions are discussed in further detail later.

The calculation is begun with an assumed displacement thickness distribution for $x_0 \leq x \leq x_1$, which is input to the boundary-layer equations. The resulting solution yields the surface pressure $C_{p,DB}$ from equation (7) which results from the inviscid flow over the displacement body. The displacement body coordinate y_{DB} is given by

$$y_{DB} = y_B + \delta^* \qquad\qquad (24)$$

where y_B is the prescribed body surface. The displacement thickness can be written as

$$\delta^*(x) = \frac{1.7208\sqrt{x}}{\sqrt{R_{\infty,L}}} + \Delta(x) \tag{25}$$

where the first part is the Blasius flat-plate solution and the second part $\Delta(x)$ is the result of the nonzero pressure gradient. Since the inviscid flow is linear, the pressure on the displacement body can be written as

$$C_{p,DB} = C_{p,B} + C_{p,\Delta} + C_{p,FP} \tag{26}$$

where $C_{p,B}$ is the pressure on the prescribed surface when no viscous effects are present and is found from the direct Cauchy integral

$$C_{p,B}(x) = -\frac{2}{\pi} \int_{-\infty}^{\infty} \frac{\left(dy_B/dx'\right)dx'}{x - x'} \tag{27}$$

where the usual small-disturbance approximations have been made. It is necessary, of course, to compute $C_{p,B}$ only once. In equation (26) $C_{p,\Delta}$ is the pressure coefficient due to Δ, the deviation of the displacement thickness from that generated by a flat plate. Also, in equation (26) $C_{p,FP}$ denotes the pressure coefficient induced by a flat-plate displacement thickness, which in the present study will be approximated as

$$C_{p,FP} = 0 \tag{28}$$

This approximation, which is discussed by Van Dyke (ref. 23), is the result of second-order boundary-layer theory for the flow over a semi-infinite flat plate. Furthermore, it should be noted that the pressure gradient induced by a flat-plate displacement thickness increases as the leading edge is approached and thus, if $C_{p,FP} \neq 0$, then there is no logical point at which a downstream, relatively local interaction calculation can be initiated other than at $x_0 = 0$.

Since the boundary-layer solution is computed inversely, the iteration procedure is simplified by also solving the inviscid flow with an inverse technique. The inverse Cauchy integral relating the pressure on the displacement body to the rate of growth of the displacement body is given by

$$\frac{dy_{DB}}{dx}(x) = \frac{1}{2\pi} \int_{-\infty}^{\infty} \frac{C_{p,DB}(x')dx'}{x - x'} \tag{29}$$

Similarly, the inverse relation for the prescribed surface is given by

$$\frac{dy_B}{dx}(x) = \frac{1}{2\pi} \int_{-\infty}^{\infty} \frac{C_{p,B}(x')dx'}{x - x'} \tag{30}$$

If equation (30) is subtracted from equation (29), then from the previous discussion it follows that

$$\frac{d\Delta}{dx}(x) = \frac{1}{2\pi} \int_{-\infty}^{\infty} \frac{C_{p,\Delta}(x')dx'}{x - x'} \tag{31}$$

The end points on this integral pose a problem since the boundary-layer solution which gives $C_{p,\Delta}$ is computed only in the range $x_0 \leqq x \leqq x_1$. In the present study the lower limit on the integral in equation (31) has been replaced with x_0 and thus, the interaction is assumed negligible upstream of x_0; that is, $C_{p,\Delta} = 0$ for $x \leqq x_0$. Downstream of the interaction at $x = x_1$, it is expected that $C_{p,\Delta}$ will be small but not zero, particularly in the early stages of iteration. It is noted that since the prescribed surface returns to a flat plate as $x \to \infty$, then $C_{p,B} = C_{p,\Delta} = 0$ is the required downstream boundary condition. This boundary condition is imposed in the inviscid calculation since the boundary-layer problem is parabolic and is solved independently of a downstream boundary condition. To avoid the discontinuity which would be encountered by setting $C_{p,\Delta} = 0$ at $x = x_1$, the following extrapolation is used for $x \geqq x_1$:

$$\tilde{C}_{p,\Delta} = \frac{a_1}{x} + \frac{a_2}{x^2} + \frac{a_3}{x^3} \tag{32}$$

where $\tilde{C}_{p,\Delta}$ denotes the extrapolated value of $C_{p,\Delta}$ and the coefficients a_1, a_2, and a_3 are computed by matching equation (32) with $C_{p,\Delta}$ obtained in the boundary-layer solution at $x = x_1$. Numerical tests on the approximate treatment of the limits in equation (31) will be discussed later.

On the basis of the preceding discussion, equation (31) is rewritten as

$$\frac{d\Delta}{dx}(x) = \frac{1}{2\pi}\left[\int_{x_0}^{x_1} \frac{C_{p,\Delta}(x')dx'}{x - x'} + \int_{x_1}^{\infty} \frac{\tilde{C}_{p,\Delta}(x')dx'}{x - x'}\right] \tag{33}$$

The first integral is evaluated numerically with a third-order-accurate quadrature formula in which the singularity at $x' = x$ is isolated in the same manner as was done by Jobe and Burggraf (ref. 13). The second integration is performed analytically with equation (32). In solving equation (33) $d\Delta/dx$ is obtained at the midpoints between the grid nodes of the boundary-layer solution. Thus, Δ at the boundary-layer points $x = \xi = m\,\Delta\xi$ is then obtained to second-order accuracy from

$$\Delta_m = \Delta_{m-1} + \frac{d\Delta}{dx}\bigg|_{m-\frac{1}{2}} \Delta x + 0(\Delta x^2) \tag{34}$$

beginning at $x = x_0$ where $\Delta = \Delta_0$ which is found by solving the boundary-layer equations in Görtler variables from the leading edge with $C_{p,B}$ prescribed. Note that Δ_0 must be small since the interaction is assumed negligible upstream of $x = x_0$. As shown in figure 2 the new displacement thickness is computed from equation (25), and the resulting value is multiplied by $\sqrt{R_{\infty,L}}$ to give $\bar{\delta}^* = \sqrt{R_{\infty,L}}\delta^*$ in order to conform to the usual boundary-layer scaling. At this point in the iteration cycle a check on convergence is made which is defined in the present study as

$$\max_m \left|\bar{\delta}_m^{*\,i+1} - \bar{\delta}_m^{*\,i}\right| < 10^{-4} \tag{35}$$

where i denotes the iteration cycle. Generally, it is found that when equation (35) is satisfied, the corresponding maximum change in C_p is about 10^{-6}. Underrelaxation was used in the present calculations at the indicated points in figure 2. A relaxation factor of 0.2 was used in the calculations; several attempts were made to increase this value, but these calculations diverged.

RESULTS AND DISCUSSION

Turbulent Boundary-Layer Calculations

Calculations with the inverse boundary-layer procedure are first discussed for the turbulent flow over a flat plate in which the input displacement thickness is computed from

a direct solution of the boundary-layer equations in Görtler variables. A comparison of the skin-friction distribution obtained from the direct and inverse calculations is shown in figure 4 along with the experimental measurements of Wieghardt and Tillman (flow number 1400 in the 1968 Stanford Conference, ref. 24). The excellent agreement between the direct and inverse boundary-layer calculations is expected since the same eddy-viscosity model is used in both of these calculations. In the inverse calculations it is found that with $\Delta x = 0.025$ the deduced edge velocity deviates from unity by 5 percent, whereas with $\Delta x = 0.0125$ this error is less than 2 percent. These boundary-layer solutions are also shown in figure 4 to be in good agreement with the experimental data. The direct solution starts at the leading edge with a laminar boundary layer and transition is assumed to occur at $x = 0.001m$. The inverse calculation begins at $x = 0.087m$, the direct solution at that station being used for the upstream boundary condition. Better agreement with the data could be obtained either by using a more detailed modeling of the transition region or by using the experimental data for the starting conditions, as was done by most of the investigators in the Stanford Conference.

Further calculations were made by using the displacement thickness distributions shown in figure 5 as input conditions to the present inverse boundary-layer procedure. The resulting solutions for the skin friction and edge velocity are shown in figures 6 to 8. Figure 6 shows the large separated region computed for laminar flow with the δ^* distribution designated as case 1 in figure 5. Note that the edge velocity, and hence the pressure, shows a plateau region between separation and reattachment which is characteristic of separated flows. This laminar calculation is the same as that designated as case B in reference 21 where additional details are presented. The turbulent boundary-layer solution corresponding to this same δ^* distribution is shown in figure 7 where it is seen that separation did not occur despite the 30-percent decrease in the edge velocity. The qualitative trend here is correct since it is well known that a turbulent boundary layer requires a larger pressure rise than a laminar boundary layer before separation occurs. As a check on the solution shown in figure 7, the deduced velocity u_e was used as an input to the boundary-layer equations expressed in Görtler variables. The resulting skin-friction distribution is seen in figure 7 to be in good agreement with that obtained in the inverse solution. There is some difference in the two solutions near the point of maximum boundary-layer thickness and is probably due to a lack of resolution across the boundary layer in the direct solution.

A more severe case was computed by using the displacement thickness distribution designated as case 2 in figure 5 as the prescribed condition. The resulting skin-friction distribution is shown in figure 8 and it indicates that separation and reattachment occur for this case. It is seen that there is no difference between the solution obtained with the approximate forward-marching procedure and that found by the global iteration technique, in which the finite-difference scheme is switched in the reversed-flow region to properly account for the reversed-flow direction. In this case the magnitude of the reversed-flow

velocity is only about $0.02U_\infty$, which at least for laminar flows is quite accurately computed by the approximate forward-marching procedure, as shown in reference 21.

An attempt was made to compute the same case as a direct calculation with u_e prescribed to see whether or not a singularity exists at the separation point as in laminar flow. The preliminary results indicate that the direct solution has a much steeper skin-friction gradient near separation, although further grid refinements as well as analysis are needed to determine the precise behavior in this region. Furthermore, the significance of this study is unclear since the solution behavior near separation will depend on the turbulent formulation, which is quite approximate in the present paper.

Laminar Viscous-Inviscid Interaction

The prescribed surface, for which interaction calculations are presented, is given by

$$y_B = t \text{ sech } 4(x - 2.5) \tag{36}$$

where $t = -0.03$ in figure 9 and $t = -0.015$ in figure 12. For these results $x_0 = 1.0$, $x_1 = 4.0$, and $\Delta x = 0.025$ which results in 121 grid points in the x-direction. The Reynolds number based on free-stream conditions and the distance from the leading edge to the assumed start of the interaction is $R_{\infty,L} = 8 \times 10^4$. In the boundary-layer calculation 87 points were used across the viscous layer; thus, a total of 10 527 grid points were used which were found to require approximately 25 sec on the CDC 6600 computer to complete one iteration cycle shown in figure 2. The results shown in figure 9 were obtained with a relatively crude initial guess on δ^* as seen in figure 10 and were found to require 64 iterations to meet the convergence criterion given in equation (35). No attempt was made to optimize the convergence rate of these calculations.

In the lower part of figure 9 the deduced displacement body is shown in comparison with the prescribed body. The points S and R refer to the separation and reattachment points, respectively, and are connected by the dividing streamline which separates the inner recirculating flow from the outer, forward flow. The displacement thickness distribution is better seen in figure 10 where the initial and final distributions are compared with the Blasius flat-plate solution. A comparison of the pressure distributions on the displacement and prescribed body shapes is shown in the upper part of figure 9. The difference in these two curves is $C_{p,\Delta}$, which is about half of the uninteracted pressure level at the bottom of the trough; this shows the large influence the boundary layer exhibits in this flow field. It is observed that $C_{p,\Delta}$ approaches zero as both the upstream and downstream boundaries are approached, which indicates that the interaction is adequately contained in this region. Additional calculations were made to insure that the results are independent of x_0, x_1, and the extrapolation given in equation (32), provided that these

boundaries are placed sufficiently far from the bottom of the trough. As a further numerical test the grid spacing in the x-direction was reduced from 0.025 to 0.0125; the results of these two calculations differ only slightly. From previous studies (ref. 6) the grid spacing across the boundary layer is considered sufficiently small and thus, the results shown in figures 9 and 10 are considered an accurate solution of the governing partial differential equations.

The skin-friction distribution for this case is shown in figure 11 along with the Blasius flat-plate distribution and that obtained by a direct calculation of the boundary-layer equations with the inviscid pressure distribution prescribed. This latter calculation demonstrates the usual singularity at separation where the slope of the skin-friction curve is infinite, whereas the solution obtained including interaction has a large but finite gradient at separation. The column iterative procedure used in the direct calculation no longer converges downstream of the separation point. As expected, the point of separation is predicted further downstream when the effects of interaction are included since the boundary layer reduces the adverse pressure gradient and thus delays separation. It is observed that the gradient is even larger near reattachment and is followed by an overshoot of the flat-plate result which is characteristic of the usual neck region downstream of a separated flow. Comparison of figures 10 and 11 shows that the maximum in skin friction corresponds to the minimum in displacement thickness in the neck region.

The results of an additional calculation in which $t = -0.015$ in equation (36) are presented in figures 12 and 13. Comparison of these results with those discussed previously for $t = -0.03$ show that the shallower trough results in a smaller but not negligible viscous-inviscid interaction. In figure 13 it is seen that for this case the inclusion of the viscous-inviscid interaction relieves the adverse pressure gradient such that the flow remains attached, despite the prediction of separation from a first-order boundary-layer calculation using the inviscid pressure distribution which is given in figure 12.

CONCLUDING REMARKS

In the present paper a technique is demonstrated for solving laminar and turbulent separated boundary layers. The turbulent separation results appear qualitatively correct; however, the quantitative accuracy of this solution technique must be evaluated by making comparisons with experimental data. It is anticipated that modifications of the eddy-viscosity model used in the present study will be required.

A new viscous-inviscid interaction procedure for separated flows is discussed and several calculations using this technique are presented. This iterative procedure requires none of the smoothing techniques usually required in numerically matching a boundary-layer and inviscid flow solution. Further studies are needed to optimize the efficiency of this interaction procedure.

REFERENCES

1. Werle, M. J.; and Vatsa, V. N.: New Method for Supersonic Boundary-Layer Separations. AIAA J., vol. 12, no. 11, Nov. 1974, pp. 1491-1497.

2. Dwoyer, D. L.: Supersonic and Hypersonic Two-Dimensional Laminar Flow Over a Compression Corner. AIAA Computational Fluid Dynamics Conference, July 1973, pp. 69-83.

3. Carter, James E.: Numerical Solutions of the Navier-Stokes Equations for the Supersonic Laminar Flow Over a Two-Dimensional Compression Corner. NASA TR R-385, 1972.

4. Bertke, S. D.; Werle, M. J.; and Polak, A.: Finite Difference Solutions to the Interacting Supersonic Turbulent Boundary Layer Equations, Including Separation Effects. Rep. No. AFL-74-4-9 (Contract N00019-73-C-0223), Dep. of Aerosp. Eng., Univ. of Cincinnati, Apr. 1974.

5. Catherall, D.; and Mangler, K. W.: The Integration of the Two-Dimensional Laminar Boundary-Layer Equations Past the Point of Vanishing Skin Friction. J. Fluid Mech., vol. 26, pt. 1, Sept. 1966.

6. Carter, James E.: Solutions for Laminar Boundary Layers With Separation and Reattachment. AIAA Paper No. 74-583, June 1974.

7. Kuhn, Gary D.; and Nielsen, Jack N.: Prediction of Turbulent Separated Boundary Layers. AIAA Paper No. 73-663, July 1973.

8. Klineberg, John M.; and Steger, Joseph L.: On Laminar Boundary-Layer Separation. AIAA Paper No. 74-94, Jan.-Feb. 1974.

9. Klineberg, John M.; and Steger, Joseph L.: Calculation of Separated Flows at Subsonic and Transonic Speeds. Proceedings of the Third International Conference on Numerical Methods in Fluid Mechanics, Volume II. Volume 19 of Lecture Notes in Physics, Henri Cabannes and Roger Temam, eds., Springer-Verlag, 1973, pp. 161-168.

10. Tai, Tsze C.: Transonic Laminar Viscous-Inviscid Interaction Over Airfoils. AIAA Paper No. 74-600, June 1974.

11. Briley, W. R.; and McDonald, H.: Numerical Prediction of Incompressible Separation Bubbles. Rep. N110887-3, United Aircraft Corp., June 1974.

12. Murman, Earll M.; and Cole, Julian D.: Calculation of Plane Steady Transonic Flows. AIAA J., vol. 9, no. 1, Jan. 1971, pp. 114-121.

13. Jobe, C. E.; and Burggraf, O. R.: The Numerical Solution of the Asymptotic Equations of Trailing Edge Flow. Proc. Roy. Soc. London, Ser. A, vol. 340, no. 1620, Sept. 3, 1974, pp. 91-111.

14. Melnik, R. E.; and Chow, R.: Asymptotic Theory of Two-Dimensional Trailing-Edge Flows. Aerodynamic Analyses Requiring Advanced Computers, Part I, NASA SP-347, 1975, pp. 177-249.

15. Stewartson, K.: On the Flow Near the Trailing Edge of a Flat Plate II. Mathematika, vol. 16, June 1969, pp. 106-121.

16. Stevens, W. A.; Goradia, S. H.; and Braden, J. A.: Mathematical Model for Two-Dimensional Multi-Component Airfoils in Viscous Flow. NASA CR-1843, 1971.

17. Bauer, Frances; and Garabedian, Paul: Computer Simulation of Shock Wave Boundary Layer Interaction. Commun. Pure & Appl. Math., vol. 26, no. 5/6, Sept./Nov. 1973, pp. 659-665.

18. Blottner, F. G.: Variable Grid Scheme Applied to Turbulent Boundary Layers, Comput. Methods Appl. Mech. & Eng., vol. 4, no. 2, Sept. 1974, pp. 179-194.

19. Harris, Julius, E.: Numerical Solution of the Equations for Compressible Laminar, Transitional, and Turbulent Boundary Layers and Comparisons With Experimental Data. NASA TR R-368, 1971.

20. Keller, Herbert B.; and Cebeci, Tuncer: Accurate Numerical Methods for Boundary-Layer Flows. II: Two-Dimensional Turbulent Flows. AIAA J., vol. 10, no. 9, Sept. 1972, pp. 1193-1199.

21. Carter, James E.; and Wornom, Stephen F.: A Forward Marching Procedure for Separated Boundary-Layer Flows. AIAA J., vol. 13, no. 8, 1975. (To be published.)

22. Reyhner, T. A.; and Flügge-Lotz, I.: The Interaction of a Shock Wave With a Laminar Boundary Layer. Int. J. Non-Linear Mech., vol. 3, no. 2, June 1968, pp. 173-199.

23. Van Dyke, Milton: Perturbation Methods in Fluid Mechanics. Academic Press, Inc., 1964.

24. Coles, D. E.; and Hirst, E. A., eds.: Computation of Turbulent Boundary Layers — 1968. AFOSR-IFP-Stanford Conference. Volume II — Compiled Data. Stanford Univ., c.1969.
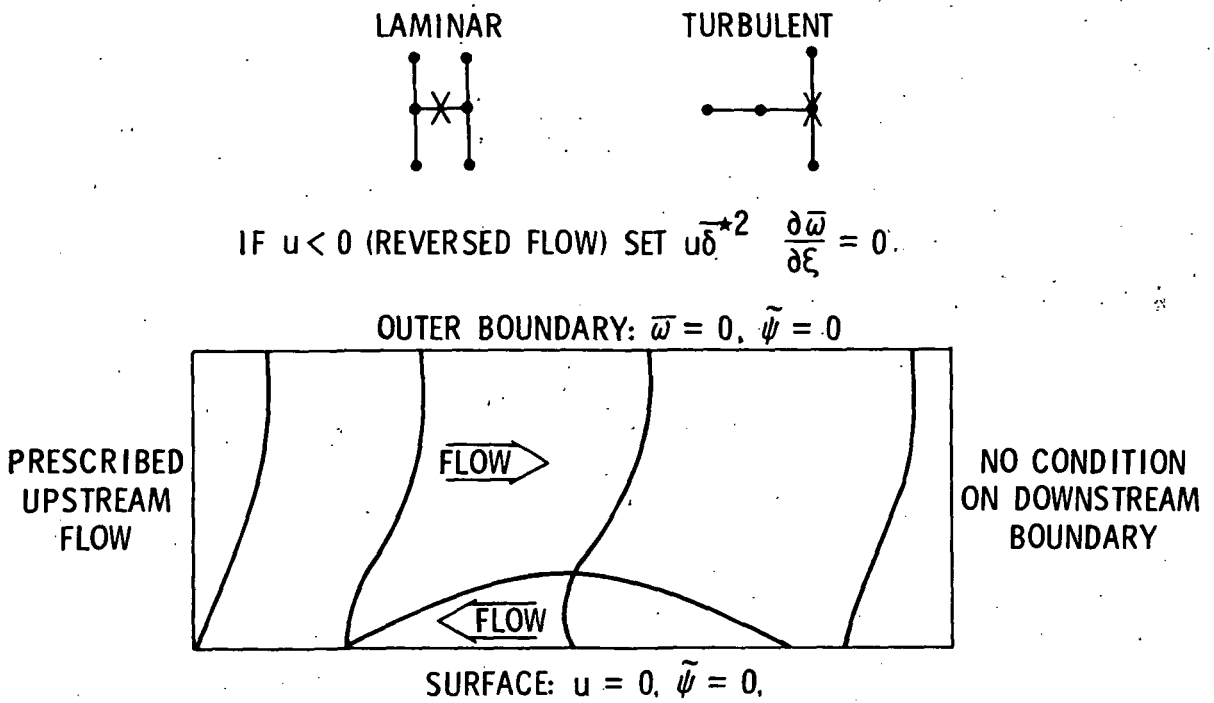
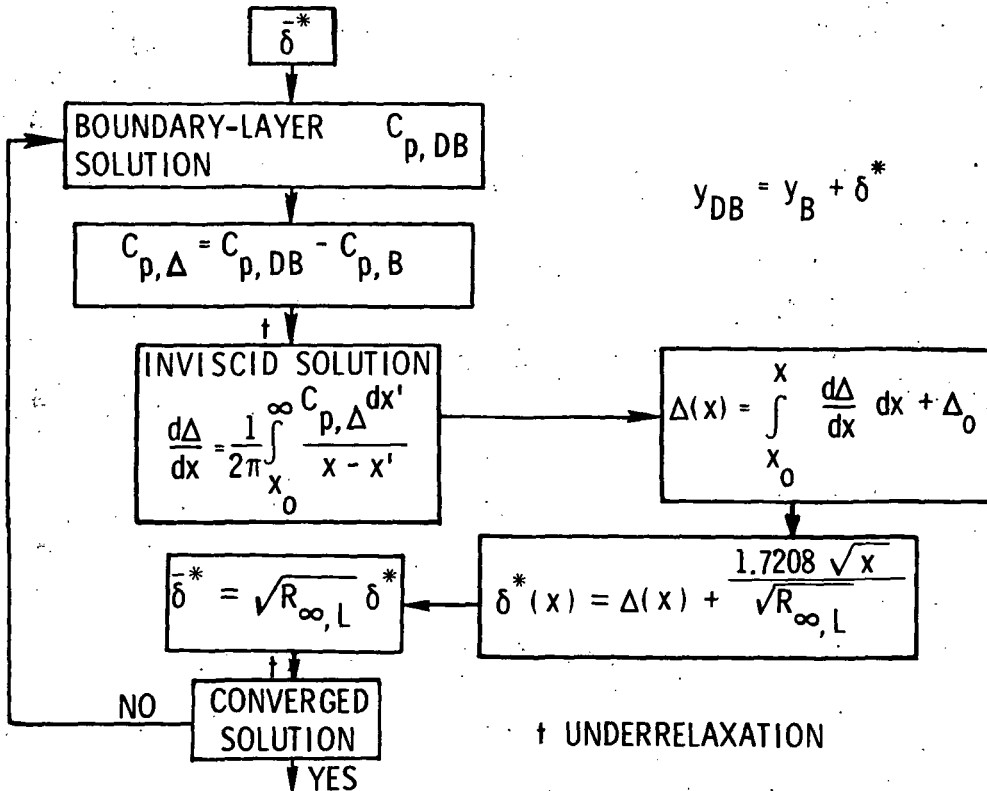Figure 1.- Boundary-layer computational schemes and boundary conditions.

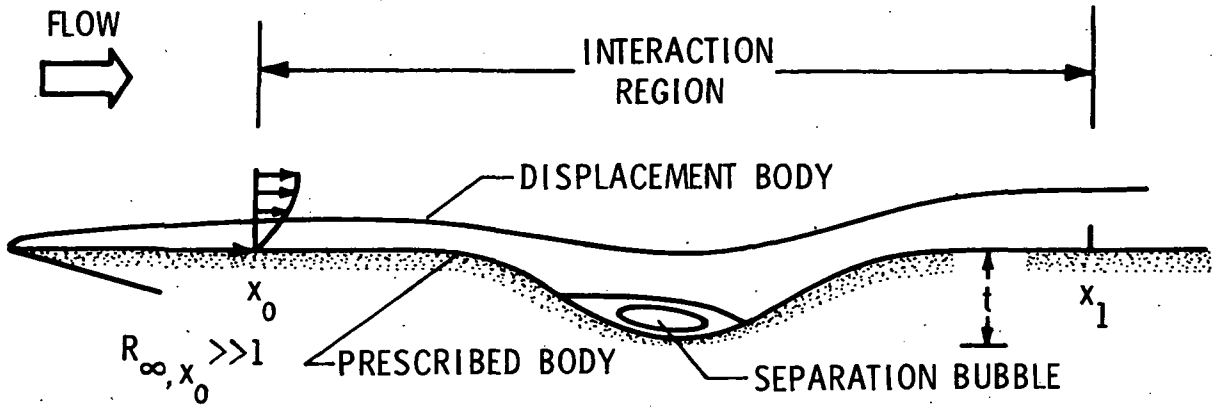Figure 2.- Inverse viscous-inviscid interaction procedure.

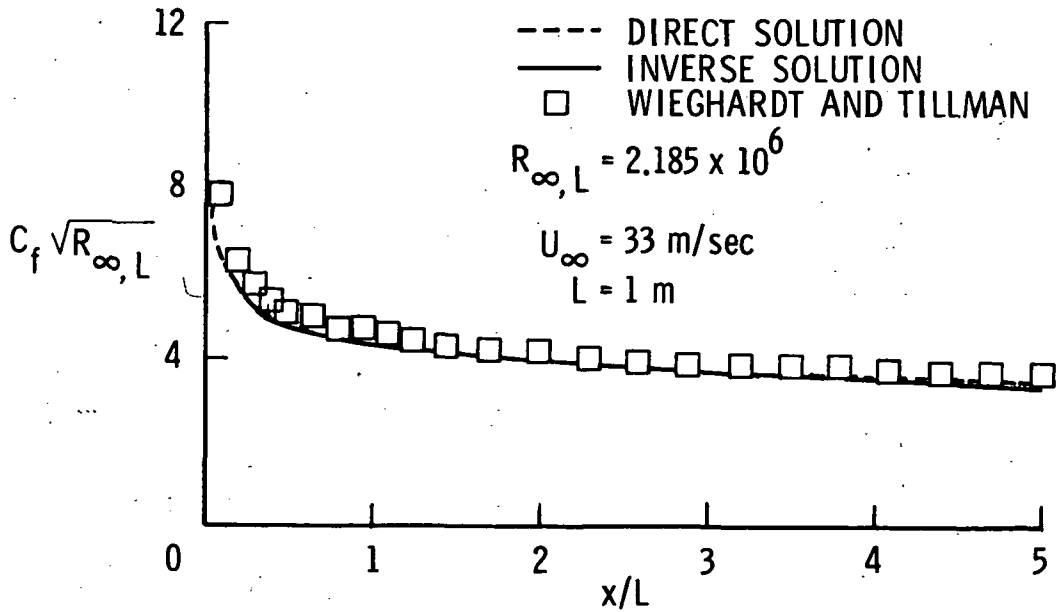Figure 3.- Schematic diagram of interaction region.
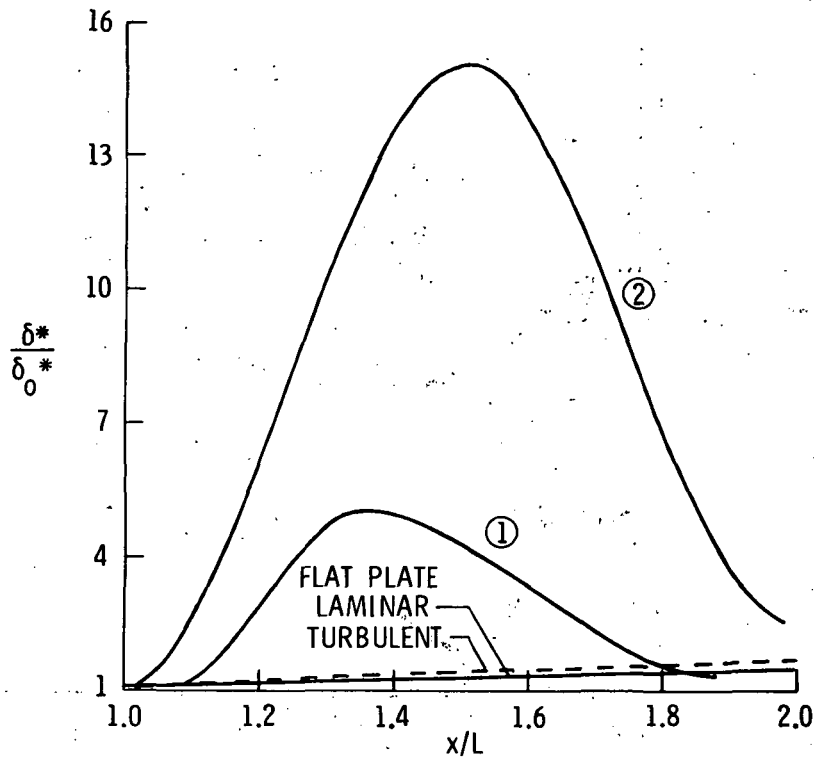

Figure 4.- Flat-plate skin-friction comparisons.
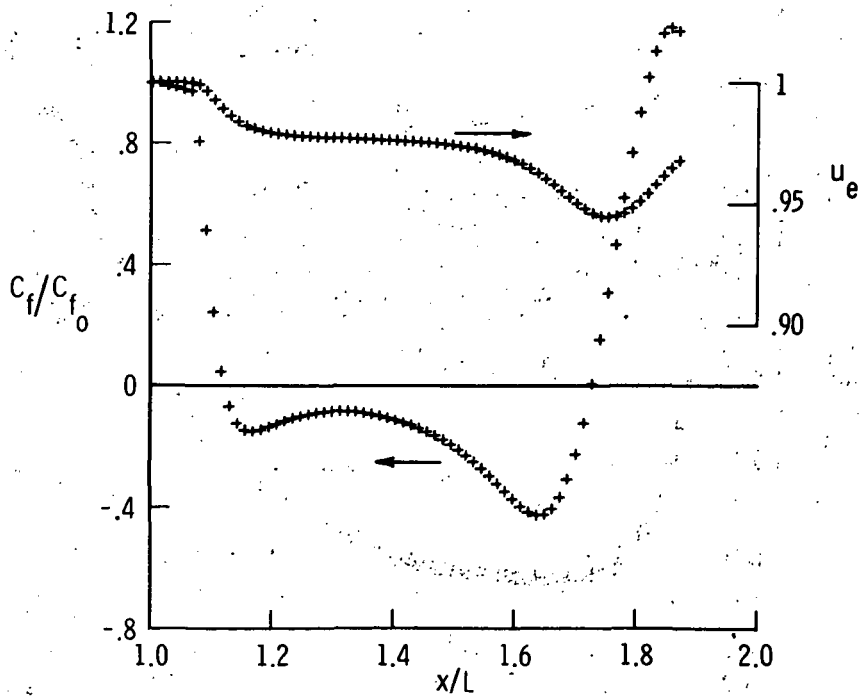
Figure 5.- Prescribed displacement thickness.

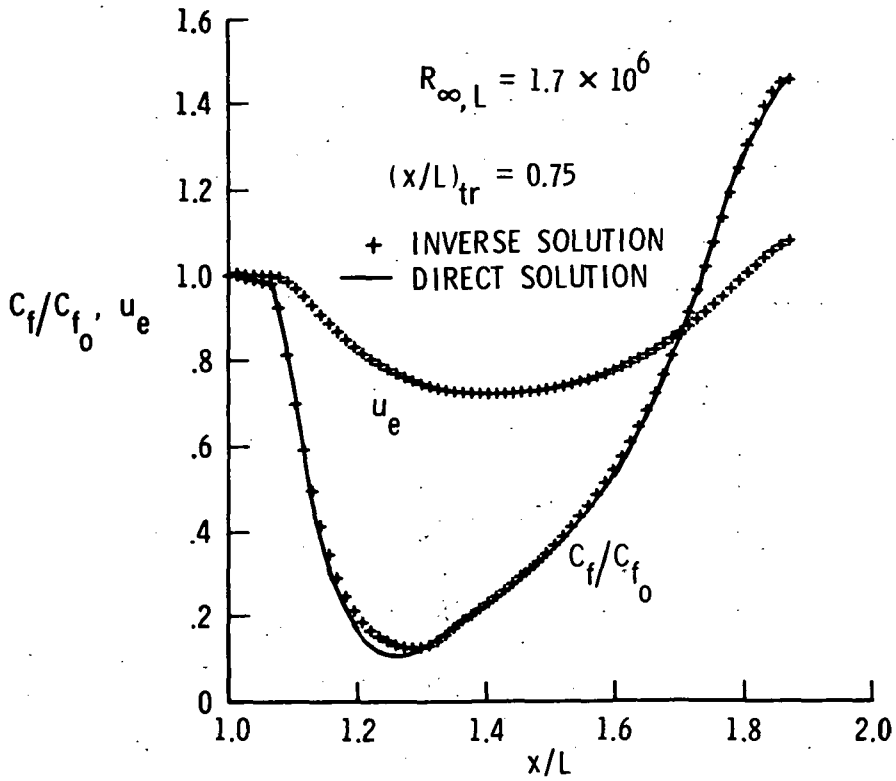Figure 6.- Skin friction and edge velocity for case 1 — laminar flow.

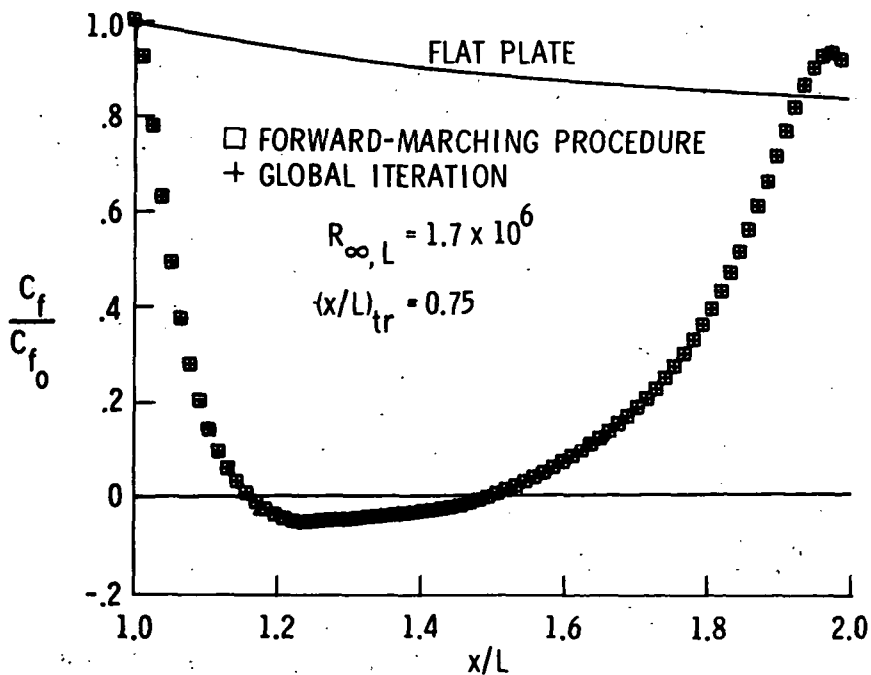**Figure 7.- Skin friction and edge velocity for case 1 — turbulent flow.**

Figure 8.- Skin friction for case 2 — turbulent separation and reattachment.
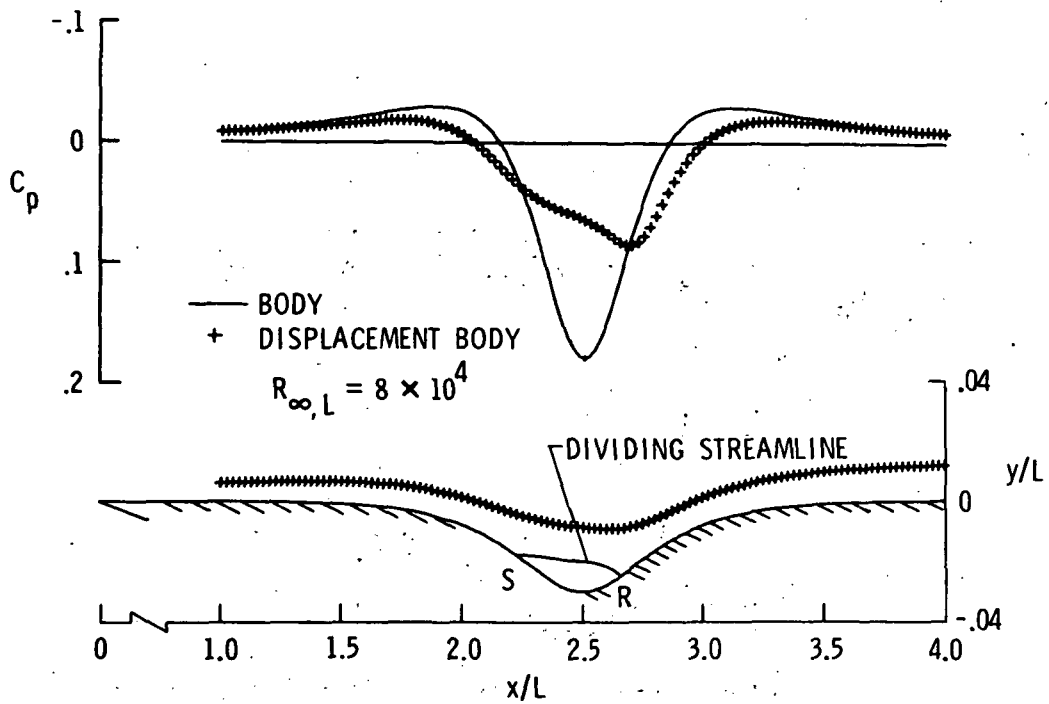
Figure 9.- Laminar viscous-inviscid interaction results; t = -0.03.
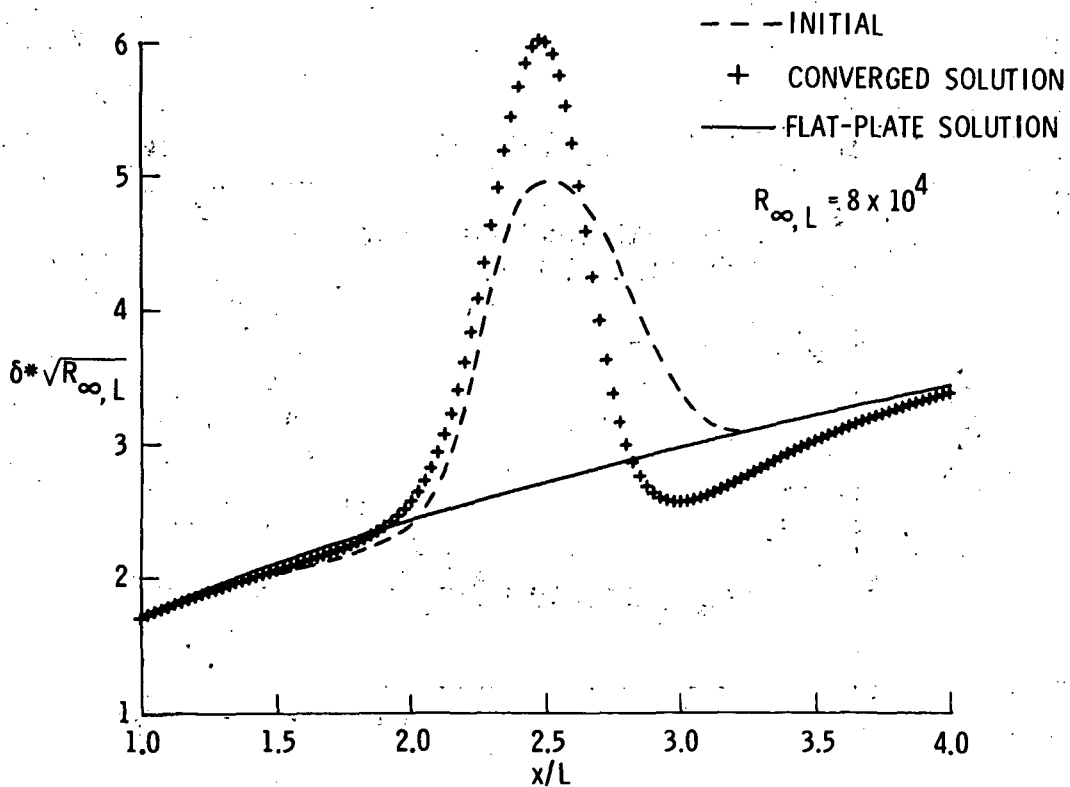
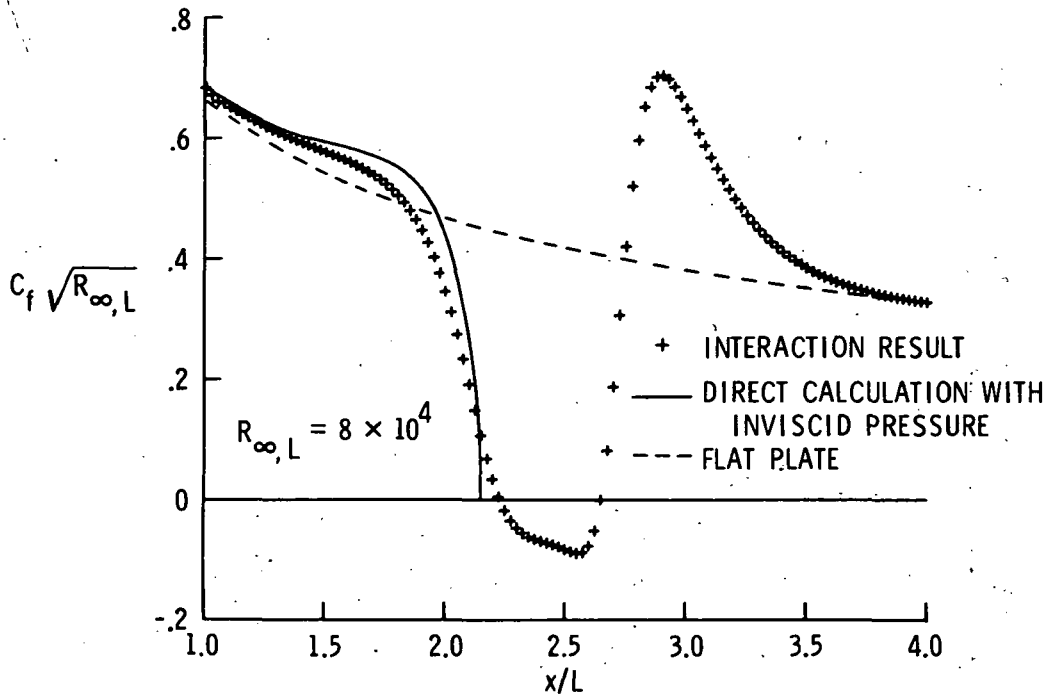Figure 10.- Initial and final displacement thickness distributions; t = -0.03.

148

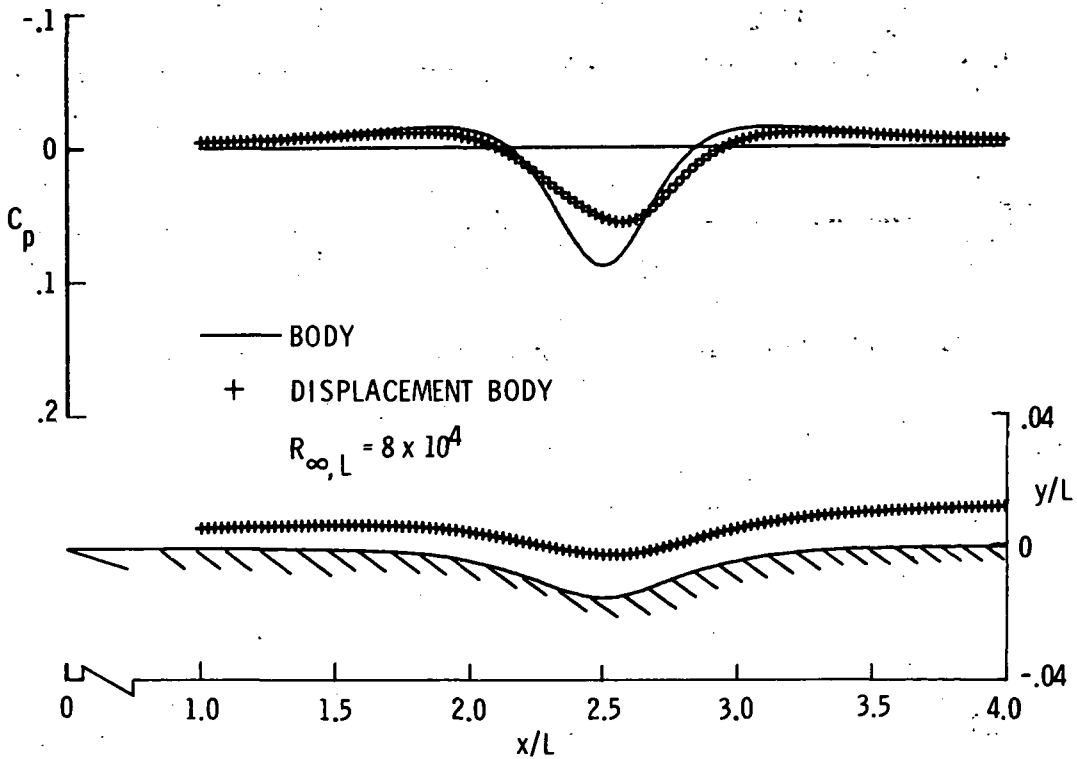Figure 11.- Laminar interaction skin friction; t = -0.03.

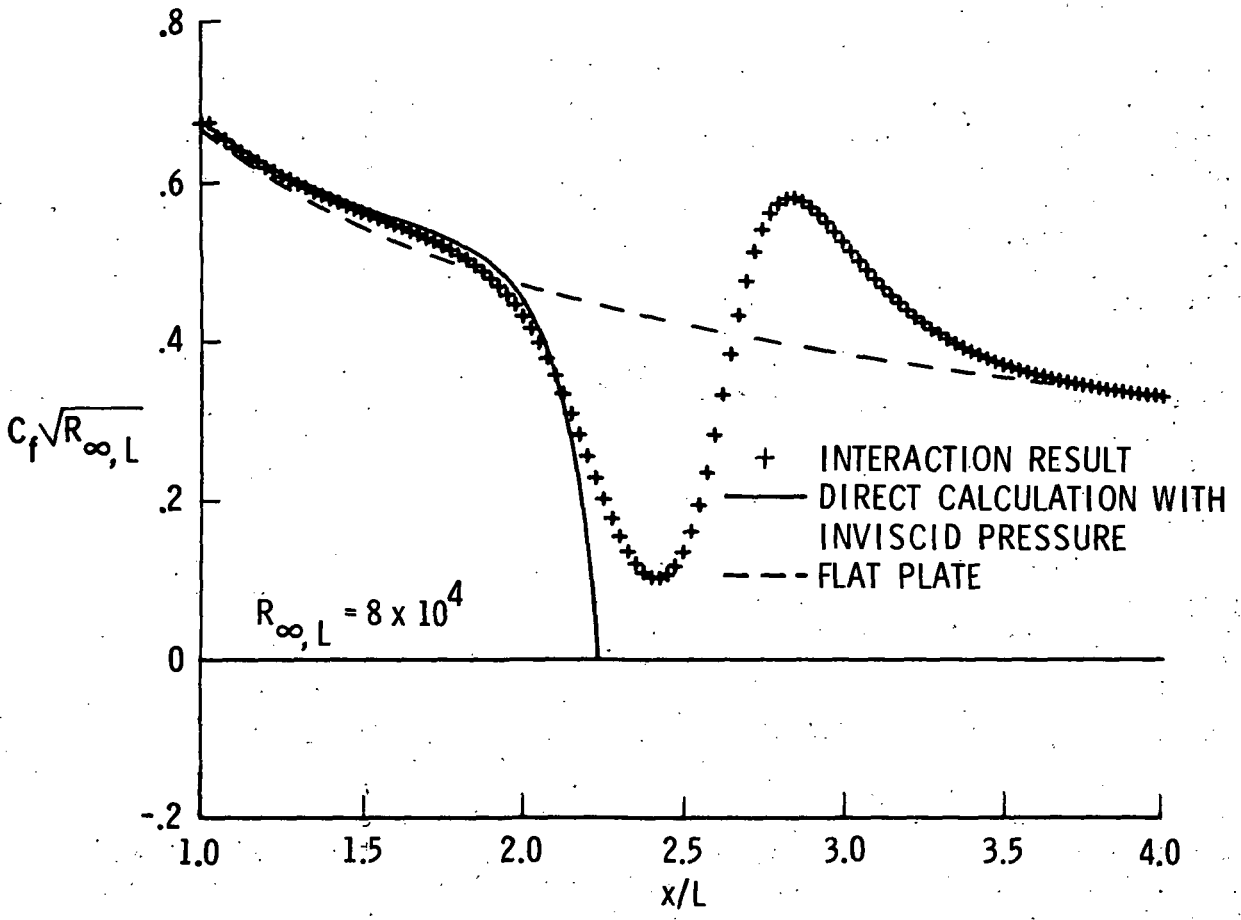Figure 12.- Laminar viscous-inviscid interaction results; t = -0.015.

149

Figure 13.- Laminar interaction skin friction; $t = -0.015$.